Field evidence for the upwind velocity shift at the crest of low dunes

P. Claudin[♯], G.F.S. Wiggs[★] and B. Andreotti[♯]

[♯] Laboratoire de Physique et Mécanique des Milieux Hétérogènes (PMMH),
UMR 7636 CNRS – ESPCI – Univ. Paris Diderot – Univ. P.M. Curie, 10 Rue Vauquelin, 75005 Paris, France.
[★] School of Geography and the Environment,
Oxford University Centre for the Environment, South Parks Road, Oxford OX1 3QY, United Kingdom.

Wind topographically forced by hills and sand dunes accelerates on the upwind (stoss) slopes and reduces on the downwind (lee) sides. This secondary wind regime, however, possesses a subtle effect, reported here for the first time from field measurements of near-surface wind velocity over a low dune: the wind velocity close to the surface reaches its maximum *upwind* of the crest. Our field-measured data show that this upwind phase shift of velocity with respect to topography is found to be in quantitative agreement with the prediction of hydrodynamical linear analysis for turbulent flows with first order closures. This effect, together with sand transport spatial relaxation, is at the origin of the dune instability mechanism.

1. Introduction

Field studies of desert dune dynamics commonly focus on investigating feedback mechanisms between topography, windflow forcing, spatial and temporal dynamism in sand flux, and resulting erosion/deposition at the surface [Lancaster at al. , 1996; Wiggs et al. , 1996; McKenna-Neuman et al. , 1997; Baddock et al. , 2011; Wiggs and Weaver , 2012]. Such studies have endeavoured to model the contemporary mechanics of simple dune shapes (with an emphasis on barchanoid forms) from fluid mechanics principles. However, progress in our understanding has been hampered by measurement complications resulting from the distortion of flow due to velocity acceleration and the practical difficulty of measuring shear velocity u_* within the near-surface inner-layer [Jackson and Hunt , 1975] where changes in shear stress are assumed to be significant for sand flux [Livingstone et al. , 2007]. Further, there is the conceptual difficulty in applying linear fluid mechanics analysis (Jackson and Hunt [1975]; Sykes [1980]; Hunt et al. [1988], see also review by Belcher and Hunt [1998]) to dune topographies that are relatively steep and incorporate a brink. Such topography forces flow separation and generates turbulent fields that lie beyond the strict applicability of the linear theory [Richards and Taylor , 1981; Buckles et al. , 1984; Finnigan et al. , 1990; Henn and Sykes , 1999; Zilker and Hanratty , 1979].

In contrast, modellers have approached the question of dune dynamics from the perspective of theoretical physics, with identification and description of the different physical ingredients necessary to reproduce dunes of different shapes [Kroy et al. , 2002; Hersen , 2004; Kroy et al. , 2005; Durán et al. , 2010]. Research on the linear stability analysis of a flat sand bed submitted to a constant wind [Andreotti et al.

, 2002; Elbelrhiti et al. , 2005; Claudin and Andreotti , 2006; Narteau et al. , 2009] has revealed the importance of two key mechanisms that must occur in the case of flow over topography. These are, (i) the upwind phase shift of the point of maximum basal shear stress with respect to dune topography and, (ii) the spatial lag in sand transport response to changing shear stress (termed 'saturation length' L_{sat}, Sauermann et al. [2001]; Andreotti et al. [2002]). These theoretical approaches are similar to those employed in subaqueous research on ripples and dunes [Kennedy , 1963; Engelund , 1970; Fredsøe , 1974; Engelund and Fredsøe , 1982; Richards , 1980; McLean , 1990; Colombini , 2004; Fourrière et al. , 2010].

The advantage garnered by the analytical modelling approach is that research effort is directed towards the initiation of dunes from flat surfaces, rather than toward understanding the mechanics of existing dune morphologies, as is the case with the geomorphological field studies. In this way, the modelling approach stays within the applicable limits of the linear theory, at least in the initial stages of dune development. The two key mechanisms of the upwind phase shift in velocity and the spatial sand flux lag have been largely overlooked in geomorphological field studies which have focussed on mature dune forms, which do not conform to the linear analysis. Further, geomorphological field studies have tended to focus on the measurement of broad windflow patterns at the dune-scale (establishing flow acceleration patterns, for example) rather than the subtle intricacies of the sub-metre scales of the hydrodynamic phase shift and sand flux lag.

A single wind tunnel investigation has suggested that the sand flux lag is of the order of a meter [Andreotti et al. , 2010] but there is no measured value available for the hydrodynamic phase shift of basal shear stress in the aeolian case. Some measurements are available in the subaqueous environment from flumes (e.g. Frederick and Hanratty [1988]; Zilker et al. [1977]) although these are in the transitional regime between laminar and turbulent flow. Numerical calculations of the phase shift are also in this transitional regime [de Angelis et al. , 1997; Cherukat et al. , 1998; Salvetti et al. , 2001; Yoon et al. , 2009]. Only one in-direct measurement of basal shear stress (established from velocity data) is available in the fully turbulent regime but this is also derived from the subaqueous environment [Poggi et al. , 2007]. Data investigating the structure of the flow over topography are available for the aeolian environment but these are all restricted to the non-linear regime (eg. Taylor et al. [1987]; Gong and Ibbetson [1989]; Gong et al. [1996]; Finnigan et al. [1990]).

In this letter we present the first field evidence of the existence of the phase shift of the point of maximum wind speed upwind of a dune crest. The experiment is carried out on a low dune with a dome topography in order to remain within the linear regime but in fully turbulent conditions. Together with data on the spatial relaxation of sand transport in response to wind velocity variations (L_{sat}) our measurements substantiate these key controls at the origin of the dune instability and initiation mechanism.

2. Field site and data collection

Our study dune was a 1.5 m high and 30 m long dome dune located on the western edge of the erg Oriental near Merzouga, eastern Morocco (31°03.103 N, 04°00.133 W). The study dune was to the south of a large star dune complex [Benalla et al. , 2003] and the surrounding landscape consisted of low, flat sand surfaces which were dry and devoid of vegetation. The dune sand had an average particle size of 310 microns as determined by laser granulometry with the upwind surface consisting of poorly sorted gravel in a sand matrix (grain size is mostly distributed in the range 200–500 microns).

We established 15 measurement sites along the centre-line of the dune parallel to a wind blowing from a compass bearing of 74° between 10.00 hrs and 14.00 hrs on 23/4/2011. In order to capture the subtle variations in velocity that we were expecting in the crest area of the dune, sites here were established at 0.5 m intervals whereas sites on both the extreme upwind and downwind flanks of the dune were established at between 1 and 8 m intervals. The topography of the centre-line of the dune was surveyed using standard levelling techniques to an accuracy of approximately 1 cm with surveyed points coinciding with the established measurement sites.

At each site small brochette sticks were inserted vertically into the sand to act as erosion pins with the height of exposed pin measured both at the beginning and end of the experiment with a tape measure. These measurements provided data on the amount of erosion or deposition evident on the dune surface during the 4 hours of the experiment and, when integrated over the distance between pins, provided an assessment of sand flux.

Two anemometer arrays were deployed, each consisting of 3 switching cup anemometers (Vector A-100R; accuracy 0.1 m/s, distance constant 2.3 m) at heights of 0.11 m, 0.30 m and 0.50 m. These heights were chosen to coincide with the airflow zones within, at and above the calculated inner-layer depth (see Section 3 below). Each anemometer array was sampled every 30 s with data recorded by Campbell CR10X dataloggers. In analysis the velocity data were averaged over a 10 minute period. These measurements provided data at the relevant timescales of turbulence both at the dune scale (30 s) and at the atmospheric scale (10 min) capturing the lower frequency turbulent structures in the boundary layer [Durán et al. , 2011].
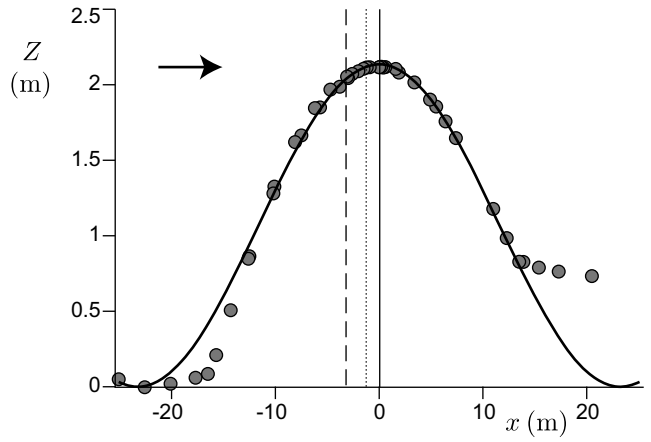
A reference site was established at the crest of the dune at which an anemometer array was permanently stationed throughout the duration of the experiment. During the 4 hrs of the experiment the wind conditions at the reference site at a height of 0.5 m peaked at 12.1 m/s with an average of 7.7 m/s. The second (mobile) array was erected at each measurement site in turn for a period of 10 minutes. Wind velocity data gained from the mobile array were then normalised by data measured at the same height and time at the reference array, denoted U_b, U_m and U_t from bottom to top respectively.

3. Results and analysis

The elevation profile of the dune on which wind velocity and erosion rates were measured is shown in Fig. 1. Although the entire surface profile is not sinusoidal, for the sake of simplicity the shape of the dune itself can be approximated by

$$Z(x) = Z_{\text{ref}} + \zeta \cos(kx), \qquad (1)$$

where $x = 0$ is the position of the dune crest. The arbitrary reference level Z_{ref} is here chosen such that $Z = 0$ at the upstream foot of the dune. Fitting this function to the

Figure 1. Dune elevation profile $Z(x)$. Wind is blowing from left to right (arrow). Symbols: measured data. Thick solid line: sinusoidal fit (Eq. 1). Several vertical lines are displayed for reference in all figures. Solid line: position of dune crest ($x = 0$). Dashed line: position of maximum velocity close to the surface (see Fig. 2). Dotted line: position of vanishing erosion rate (see Fig. 4).

data gives an effective wavenumber $k \simeq 0.14$ m^{-1} (i.e. a wavelength $\lambda = 2\pi/k \simeq 46$ m) and an amplitude $\zeta \simeq 1.1$ m. The dune aspect ratio $2\zeta/\lambda \simeq 0.05$ means the topography is at approximately the upper limit for the hydrodynamical linear regime to be valid. The thinkness of the inner layer ℓ of the dune can be estimated with [Taylor et al. , 1987]:

$$\frac{\ell}{\lambda} \frac{1}{\kappa^2} \ln^2 \frac{\ell}{z_0} = \mathcal{O}(1). \qquad (2)$$

$\kappa \simeq 0.4$ is the von Kármán constant. The hydrodynamical roughness z_0, due to the presence of a transport layer or of aeolian ripples, is typically on the order of a fraction of a millimeter. As a consequence, the thickness ℓ for a dune of this size ($\lambda \simeq 46$ m) is expected to be in the range 15–20 cm.

We display in Fig. 2 the longitudinal profile of the relative wind velocity measured with the bottom anemometer at 11 centimeters above the surface u_b/U_b, i.e. *within the inner layer*. Consistently, with the linear analysis, this profile can also be fitted by a sinusoidal function of the same wave number k as for the dune elevation, i.e. of the form:

$$u_b(x) = u_b^0 + \delta u_b \cos(kx + \varphi_b). \qquad (3)$$
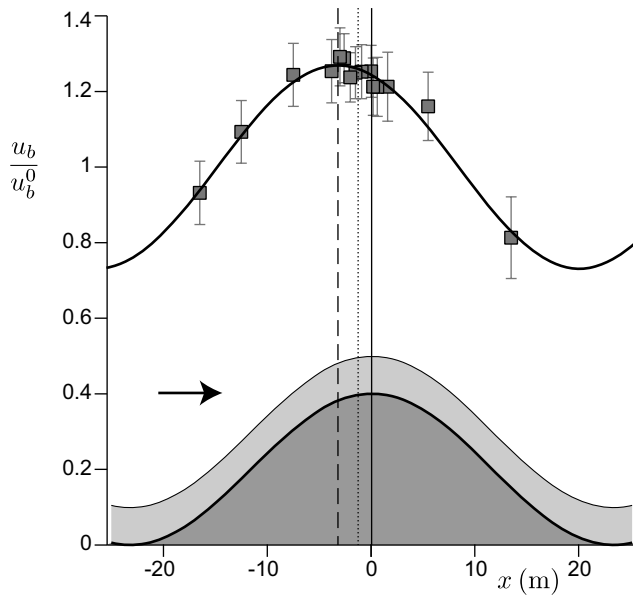
Importantly, Z and u_b are not in phase: the velocity reaches its maximum upstream of the crest. Here the phase difference is $\varphi_b \simeq 0.43$, i.e. around 26°, or $\varphi_b/k \simeq 3.2$ m upwind (vertical dashed lines in figures). The two other fitting parameters are $u_b^0/U_b \simeq 0.8$ and $\delta u_b/u_b^0 \simeq 0.27$.

Assuming that the logarithmic law of the wall locally holds in the inner layer at each position x, the velocity can then be used as a proxy to calculate the basal shear stress with $\tau_b \propto \rho_f u_b^2$, where ρ_f is the density of the air. At the linear order, we can write:

$$\tau_b(x) \propto \rho_f (u_b^0)^2 \left[1 + k\zeta \left(\mathcal{A} \cos(kx) - \mathcal{B} \sin(kx) \right) \right], \qquad (4)$$

where $\mathcal{A}$ and $\mathcal{B}$ are given by

$$\mathcal{A} = 2 \frac{\delta u_b}{u_b^0} \cos \varphi_b \frac{1}{k\zeta} \quad \text{and} \quad \mathcal{B} = 2 \frac{\delta u_b}{u_b^0} \sin \varphi_b \frac{1}{k\zeta}. \qquad (5)$$
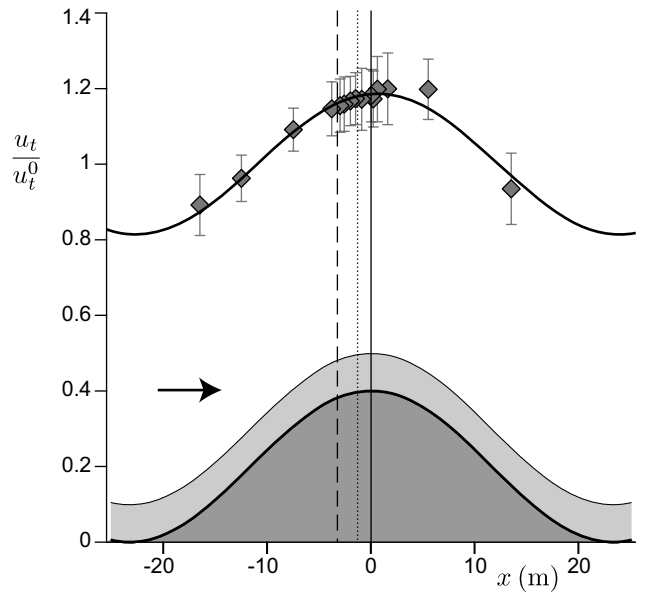
Figure 2. Longitudinal profile of the wind velocity u_b at 11 cm above the surface. Symbols: measured data. Thick solid line: sinusoidal fit (Eq. 3). Vertical reference lines: same legend as in Fig. 1. In particular, the position at which the fitted line is maximum is marked with the dashed line. At the bottom: sketch of the dune topography (dark grey) and of the inner layer (light grey) within which the anemometer was located in this case.
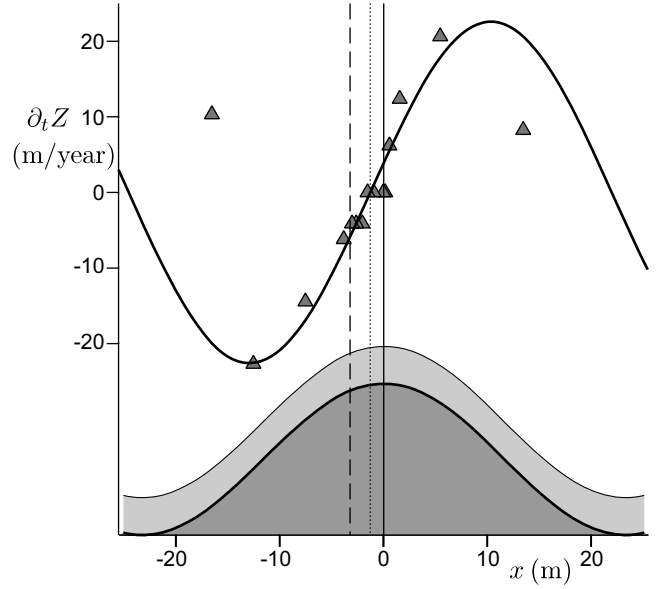

Figure 3. Longitudinal profile of the wind velocity u_t at 50 cm above the surface, i.e. above the inner layer. Symbols: measured data. Thick solid line: sinusoidal fit. Vertical reference lines: same legend as in Fig. 1.

Figure 4. Longitudinal profile of the erosion rate $\partial_t Z$. Symbols: data measured with erosion pins. Thick solid line: sinusoidal fit. Vertical reference lines: same legend as in Fig. 1. In particular, the position at which the fitted line vanishes is marked with the dotted line.

Expression (4) is formally very general, while (5) is specific to the approximation used here to relate τ_b to u_b. In fact, since sediment transport is controlled by the basal shear stress, these two parameters $\mathcal{A}$ and $\mathcal{B}$ are all what is needed as hydrodynamical inputs in bedform models, and are therefore of fundamental importance for the understanding of the dune instability mechanism.

With the different values of the parameters deduced from the fitting of the elevation and velocity profiles, we numerically get $\mathcal{A} \simeq 3.4 \pm 0.4$ and $\mathcal{B} \simeq 1.55 \pm 0.05$. Error bars result from the account of uncertainty in the determination of these parameters, and of the selected wavenumber k in particular. These values can be compared to linear theories that make predictions for τ_b. They can be computed in the case of a semi-infinite turbulent flow over a wavy surface, with a first order turbulent closure on the mixing length L of the rough type $L = \kappa(z + z_0)$, where z is the vertical distance to the surface [Fourrière et al. , 2010]. $\mathcal{A}$ and $\mathcal{B}$ are then found to be very weak (logarithmic) functions of kz_0. In our case, kz_0 is in the range 10^{-5}–10^{-4}, which gives $\mathcal{A} \simeq 4$ and $\mathcal{B} \simeq 2$, i.e. close to our measured values. Besides, Ayotte et al. [1994] have shown that the prediction of the basal shear stress is very robust with respect to the (arbitrary) choice of the turbulent closure. Notice that non-linearities are expected to reduce this shift.

We now focus on the effect of the vertical distance from the surface at which velocity is measured. In Fig. 3, we display the profile of the wind velocity measured with the upper anemometer located at 50 centimeters above the surface (u_t). In contrast with the bottom profile u_b which is phase advanced with respect to the topography, the top one u_t has a small downwind phase shift ($\varphi_t \simeq -5°$, or 0.6 m downwind). The velocity profile from the middle anemometer u_m is intermediate (not shown), with no detectable phase shift. The top anemometer is clearly located in the outer layer, where the dominant hydrodynamical mechanisms at work are different from those in the inner layer. In particular, rapid distortion and streamline curvature become important, and anisotropic second order turbulent closures are necessary to describe the flow in this region [Ayotte et al. , 1994; Finnigan et al. , 1990]. This slight phase delay in the outer layer is related to the lag between production and dissipation of turbulent fluctuations [Weng et al. , 1991;

Wiggs et al. , 1996; van Boxel et al. , 1999; Walker and Nickling , 2003].

Measured data for the erosion rate during the experiment are shown in Fig. 4. In accordance with the linear analysis, we expect this profile to have longitudinal variations as $\sin(kx + \varphi_q)$. Erosion rate and (volumetric) sand flux $q(x)$ are related through the matter conservation equation as $\partial_t Z + \partial_x q = 0$. The position at which $\partial_t Z$ vanishes then corresponds to the flux maximum. Here we find $\varphi_q \simeq 10°$ (or 1.2 m upwind, vertical dotted lines in figures), i.e. the maximum in sand flux is phase advanced to topography, but not to such a degree as velocity.

The reason why sediment flux is delayed with respect to the velocity is that sand transport does not adjust instantaneously to changes in shear stress: q relaxes towards its equilibrium value q_{sat} over a spatial scale L_{sat}, the so-called saturation length [Sauermann et al. , 2001; Andreotti et al. , 2002; Andreotti , 2004; Andreotti et al. , 2010]. These data then allow us to give an indirect estimate of L_{sat}. Following our previous studies [Andreotti et al. , 2002; Elbelrhiti et al. , 2005; Claudin and Andreotti , 2006; Andreotti et al. , 2010], we assume for this purpose an exponential behavior for this relaxation and a transport law of the form $q_{sat} = \chi(\tau_b - \tau_{th})$, where τ_{th} is the shear threshold for transport and χ a dimensionful constant. We then get:

$$ kL_{sat} = \tan(\varphi_b - \varphi_q) = \frac{\mathcal{B} - \mathcal{A}\tan\varphi_q}{\mathcal{A} + \mathcal{B}\tan\varphi_q}. \qquad (6) $$

With the above values of $\mathcal{A}$, $\mathcal{B}$ and k, we compute $L_{sat} \simeq 2$ m. Taking into account the fact that the shear threshold depends on the bed slope as $\tau_{th} = \tau_{th}^0(1 + \partial_x Z/\mu)$, where $\mu \simeq 0.6$ is the avalanche slope, Eq. 6 is modified with $\mathcal{B}$ replaced by $\mathcal{B}_\mu = \mathcal{B} - \frac{1}{\mu}\frac{\tau_{th}^0}{\tau_b^0}$. Here we take $\tau_{th}^0/\tau_b^0 \simeq (u_{th}^0/u_b^0)^2$, a ratio estimated around 0.4 during our experiment, i.e. $\mathcal{B}_\mu \simeq 0.9$. This leads to $L_{sat} \simeq 0.7$ m. Previous direct measurements of the saturation length performed by Andreotti et al. [2010] gave $L_{sat} \simeq 0.55 \pm 0.1$ m for grains of diameter $d \simeq 120$ μm (wind tunnel experiments), and $L_{sat} \simeq 1 \pm 0.2$ m for grains of diameter $d \simeq 185$ μm (field experiments). Here, as $d \simeq 310$ μm and since the saturation length is expected to be proportional to the grain size, the range into which this indirect estimate falls is fair, given the relatively low spatial resolution (0.5 m at most) with which the erosion rate profile was measured.

4. Conclusions

Our data give the first field evidence of the upwind phase shift of velocity close to the surface with respect to topography. Importantly, this shift is only observed when the velocity is measured in the inner layer: it vanishes and even changes sign (velocity maximum downwind of the dune crest) when the measurement is undertaken at greater heights above the surface. The value of this upwind phase-shift is, furthermore, in quantitative agreement with the prediction of the hydrodynamical linear analysis with first order closures for turbulent flows. In conclusion, the two ingredients of the dune instability mechanism, namely (i) the upwind phase-shift of the basal shear stress with respect to the topography and (ii) the spatial lag L_{sat} of sand transport with respect to this stress [Andreotti et al. , 2010], are now both experimentally validated.

These results are based on measurements undertaken on a single dune. More data are required on differing dune sizes and mean wind velocities. As for the erosion rate, a better space resolution and a longer time integration is needed to gain precision in the indirect estimate of L_{sat}.

Previous field tests of the predictions of Jackson and Hunt [1975] have been performed on large hills [Taylor et al. ,

1987], making the entire longitudinal profile of the velocity close to the surface difficult to record. As a result, only the overall speed-up and the general structure of the wind flow has been assessed. In the other extreme, wind tunnel studies on decimeter-scale bumps do not allow access to the inner layer, which is too small. Here we have illustrated that dunes provide good intermediate topographies over which turbulent predictions can be tested in detail. Besides, although the wind flow is influenced by sediment transport, in particular due to an increase of the aerodynamical roughness, the sandy surface of dunes is more uniform and idealized than that of vegetated environments.

References

Andreotti, B. (2004) A two species model of aeolian sand transport. *J. Fluid Mech.* **510**, 47–50.

Andreotti, B., Claudin, P. and Douady, S. (2002) Selection of dune shapes and velocities. Part 2: A two-dimensional modelling. *Eur. Phys. J. B* **28**, 341–352.

Andreotti, B., Claudin, P. and Pouliquen, O. (2010) Measurements of the aeolian sand transport saturation length. *Geomorphology* **123**, 343–348.

Ayotte, K.W., Xu, D. and Taylor, P.A. (1994) The impact of turbulence closure schemes on predictions of the mixed spectral finite-difference model for flow over topography. *Boundary-Layer Met.* **68**, 1–33.

Baddock, M.C., Livingstone, I. and Wiggs, G.F.S. (2007) The geomorphological significance of airflow patterns in transverse dune interdunes, *Geomorphology* **87**, 322–336.

Baddock, M.C., Wiggs, G.F.S. and Livingstone, I. (2011) A field study of mean and turbulent flow characteristics upwind, over and downwind of barchan dunes. *Earth Surface Processes and Landforms* **36**, 1435–1448.

Belcher, S.E. and Hunt, J.C.R. (1998) Turbulent flow over hills and waves. *Ann. Rev. Fluid Mech.* **30**, 507–538.

Benalla, M., Alem, M., Rognon, P., Desjardins, R., Hilali, A. and Khardi, A. (2003) Les dunes du Tafilalet (Maroc): dynamique éolienne et ensablement des palmeraies. *Sciences et changements planétaires/Sécheresse* **14**, 73–83.

Buckles, J., Hanratty, T.J. & Adrian, R.J. (1984) Turbulent flow over large-amplitude wavy surfaces. *J. Fluid Mech.* **140**, 27–44.

Cherukat, P., Na, Y., Hanratty, T.J. and McLaughlin, J.B. (1998) Direct numerical simulation of a fully developped turbulent flow over a wavy wall. *Theoret. Comput. Fluid Dynamics* **11**, 109–134.

Claudin, P. and Andreotti, B. (2006) A scaling law for aeolian dunes on Mars, Venus, Earth, and for sub-aqueous ripples. *Earth Pla. Sci. Lett.* **252**, 30–44.

Colombini, M. (2004) Revisiting the linear theory of sand dune formation. *J. Fluid Mech.* **502**, 1–16.

de Angelis, V., Lombardi, P. and Banerjeeb, S. (1997) Direct numerical simulation of turbulent flow over a wavy wall. *Phys. Fluids* **9**, 2429–2442.

Durán, O., Claudin, P. and Andreotti B. (2011) On aeolian transport: grain-scale interactions, dynamical mechanisms and scaling laws. *Aeolian Research* **3**, 243–270.

Durán, O., Parteli, E.J.R. and Herrmann, H.J. (2010) A continuous model for sand dunes: Review, new developments and application to barchan dunes and barchan dune fields. *Earth Surf. Processes and Landforms* **35**, 1591–1600.

Elbelrhiti, H., Claudin, C., and Andreotti, B. (2005) Field evidence for surface wave induced instability of sand dunes. *Nature* **437**, 720–723.

Engelund, F. (1970) Instability of erodible beds. *J. Fluid Mech.* **42**, 225–244.

Engelund, F. and Fredsøe, J. (1982) Sediment ripples and dunes. *Ann. Rev. Fluid Mech.* **14**, 13–37.

Finnigan, J.J., Raupach, M.R., Bradley, E.F. and Aldis G.K. (1990) A wind tunnel study of turbulent flow over a two-dimensional ridge. *Boundary-Layer Met.* **50**, 277–317.

Fourrière, A., Claudin, P. and Andreotti, B. (2010) Bedforms in a turbulent stream: formation of ripples by primary linear instability and of dunes by non-linear pattern coarsening. *J. Fluid Mech.* **649**, 287–328.

Frederick, K.A. and Hanratty, T.J. (1988) Velocity measurements for a turbulent nonseparated flow over solid waves. *Exp. Fluids* **6**, 477–486.

Fredsøe, J. (1974) On the development of dunes in erodible channels. *J. Fluid Mech.* **64**, 1–16.

Gong, W. and Ibbetson, A. (1989) A wind tunnel study of turbulent flow over model hills. *Boundary-Layer Met.* **49**, 113–148.

Gong, W., Taylor, P.A. and Dörnbrack, A. (1996) Turbulent boundary-layer flow over fixed aerodynamically rough two-dimensional sinusoidal waves. *J. Fluid Mech.* **312**, 1–37.

Henn, D.S. and Sykes, R.I. (1999) Large-eddy simulation of flow over wavy surfaces. *J. Fluid Mech.* **383**, 75–112.

Hersen, P. (2004) On the crescentic shpae of barchan dunes. Eur. Phys. J. B **37**, 507–514.

Hunt, J.C.R., Leibovich, S. and Richards, K.J. (1988) Turbulent shear flows over low hills. *Q. J. R. Meteorol. Soc.* **114**, 1435–1470.

Jackson, P.S. and Hunt, J.C.R. (1975) Turbulent wind flow over a low hill. *Q. J. R. Meteorol. Soc.* **101**, 929–955.

Kennedy, J.F. (1963) The mechanics of dunes and antidunes in erodible bed channels. *J. Fluid Mech.* **16**, 521–544.

Kroy, K., Fischer, S. and Obermayer, B. (2005) The shape of barchan dunes. *J. Phys. Cond. Matt.* **17**, S1129–S1235.

Kroy, K., Sauermann, G. and Herrmann, H.J. (2002) Minimal model for aeolian sand dunes. *Phys. Rev. E* **66**, 031302.

Lancaster, N., Nickling, W.G., McKenna Neuman and C., Wyatt, V.E. (1996) Sediment flux and airflow on the stoss slope of a barchan dune. *Geomorphology* **17**, 55–62.

Livingstone, I, Wiggs, G.F.S. and Weaver, C.M. (2007) Geomorphology of desert sand dunes. *Earth Science Reviews* **80**, 239–257.

McKenna-Neuman, C., Lancaster, N. and Nickling, W. G. (1997) Relations between dune morphology, air flow, and sediment flux on reversing dunes, Silver Peak, Nevada. *Sedimentology* **44**, 1103–1113.

McLean, S.R. (1990) The stability of ripples and dunes. *Earth-Science Rev.* **29**, 131–144.

Narteau, C., Zhang, D., Rozier, O. and Claudin, P. (2009) Setting the length and time scales of a cellular automaton dune model from the analysis of superimposed bedforms. *J. Geophys. Res.* **114**, F03006.

Poggi, D. , Katul, G.G., Albertson, J.D. and Ridolfi, L. (2007) An experimental investigation of turbulent flows over a hilly surface. *Phys. Fluids* **19**, 036601.

Richards, K.J. (1980) The formation of ripples and dunes on an erodible bed. *J. Fluid Mech.* **99**, 597–618.

Richards, K.J. and Taylor, P.A. (1981) A numerical model of flow over sand waves in water of finite depth. *Geophys. J. R. Astr. Soc.* **65**, 103–128.

Sauermann, G., Kroy, K. and Herrmann, H.J. (2001) Continuum saltation model for sand dunes. *Phys. Rev. E 64*, 031305.

Salvetti, M.V., Damiani, R. and Beux, F. (2001) Three-dimensional coarse large-eddy simulations of the flow above two-dimensional sinusoidal waves. *Int. J. Numer. Meth. Fluids* **35**, 617–642.

Sykes, R.I. (1980) An asymptotic theory of incompressible turbulent boundary-layer flow over a small bump. *J. Fluid Mech.* **101**, 647–670.

Taylor, P.A., Mason, P.J. and Bradley, E.F. (1987) Boundary-layer flow over low hills. *Boundary-Layer Met.* **39**, 107–132.

van Boxel, J.H., Arens, A.M. and van Dijk, P.M. (1999) Aeolian processes across transverse dunes. I: Modelling the air flow. *Earth Surf. Processes Landforms* **24**, 255–270.

Walker, I.J. and Nickling, W.G. (2003) Simulation and measurement of surface shear stress over isolated and closely spaced transverse dunes in a wind tunnel. *Earth Surf. Processes Landforms* **28**, 1111–1124.

Weng, W.S., Hunt, J.C.R., Carruthers, D.J., Warren, A., Wiggs, G.F.S., Linvingstone, I. and Castro, I. (1991) Air flow and sand transport over sand dunes. Acta Mechanica **2**, 1–22.

Wiggs, G.F.S., Livingstone, I. and Warren, A. (1996) The role of streamline curvature in sand dune dynamics: evidence from field and wind tunnel measurements. *Geomorphology* **17**, 29–46.

Wiggs, G.F.S. and Weaver, C.M. (2012) Turbulent flow structures and aeolian sediment transport over a barchan sand dune. *Geophys. Res. Lett.* **39** L05404.

Yoon, H.S., El-Sammi, O.A., Huynh, A.T., Chun, H.H., Kim, H.J., Pham, A.H. and Park, L.R. (2009) Effect of wave amplitude on turbulent flow in a wavy channel by direct numerical simulation. *Ocean Eng.* **36**, 697–707.

Zilker, D.P., Cook, G.W. and Hanratty, T.J. (1977) Influence of the amplitude of a solid wavy wall on a turbulent flow. Part 1. Non-separated flows. *J. Fluid Mech.* **82**, 29–51.

Zilker, D.P. and Hanratty, T.J. (1979) Influence of the amplitude of a solid wavy wall on a turbulent flow. Part 2. Separated flows. *J. Fluid Mech.* **90**, 257–271.

PMMH, UMR 7636 CNRS – ESPCI – Univ. Paris Diderot – Univ. P.M. Curie, 10 Rue Vauquelin, 75005 Paris, France. (`claudin@pmmh.espci.fr`)

School of Geography and the Environment, Oxford University Centre for the Environment, South Parks Road, Oxford OX1 3QY, United Kingdom.